Advances in Science and Technology Research Journal

Advances in Science and Technology Research Journal, 2026, 20(10), 147–156
https://doi.org/10.12913/22998624/224548
ISSN 2299-8624, License CC-BY 4.0

Received: 2026.05.26
Accepted: 2026.07.10
Published: 2026.09.01

Experimental study of the dynamic response of a dual throat fluidic thrust vectoring nozzle

Wiktor Hoffmann[1*], Magda Joachimiak[1]

[1] Faculty of Environmental Engineering and Energy, Institute of Thermal Energy, Poznan University of Technology, Piotrowo 3, 61-138 Poznan, Poland

* Corresponding author's e-mail: wiktor.hoffmann@put.poznan.pl

ABSTRACT

Dual-Throat Nozzles (DTNs) are a class of fluidic thrust vectoring nozzles in which secondary injection modifies the internal pressure distribution and deflects the primary jet. Although DTN performance has been described in the literature mainly under steady operating conditions, experimental data on transient response remain limited. The present study investigates the dynamic behavior of an axisymmetric DTN during secondary-flow actuation. Experiments were carried out on a facility supplied by a Ludwieg Tube for the primary flow and a compressed-air system for the secondary injection. Wall-pressure signals were acquired synchronously at 51.2 kS/s/ch and analyzed using Savitzky-Golay smoothing and a first-order model with delay fitted to the transient response. Under the investigated operating conditions, the measured response exhibited delayed asymptotic behavior. The dimensionless time constant was determined in order of 9. Pressure oscillations in the kilohertz range were also observed during operation, indicating non-stationary flow phenomena inside the nozzle. The results provide experimentally identified response parameters that can support reduced-order modeling, response-time prediction, and preliminary control-oriented assessment of DTN-based thrust-vectoring systems.

Keywords: dual throat nozzle, thrust vector control, first order system, dynamic response, jet propulsion.

INTRODUCTION

Thrust vector control is a key technology enabling maneuverability and stability of modern aircraft and rocket propulsion systems. By altering the direction of the exhaust jet, thrust vectoring allows vehicles to maintain control in flight regimes where aerodynamic control surfaces become ineffective, such as during high-altitude flight, vertical take-off and landing, or rapid attitude maneuvers. Traditionally, thrust vector control has been implemented using mechanical systems such as gimballed nozzles, movable exhaust flaps, or jet vanes. While effective, these solutions introduce additional mechanical complexity, structural mass, and maintenance requirements. For this reason, significant research effort has been directed toward fluidic thrust vectoring, where the direction of the primary jet is modified by injecting a relatively small secondary flow into the nozzle.

Among the fluidic thrust vectoring concepts proposed in the literature [1, 2], the DTN has attracted particular attention due to its relatively high vectoring efficiency and small thrust penalties. The DTN geometry consists of two minimum cross-sections separated by a recessed cavity inside a convergent-divergent-convergent nozzle structure. Injection of a secondary jet near the upstream throat modifies the pressure distribution in the cavity and induces asymmetric flow separation (Figure 1). As a consequence, the sonic plane becomes skewed and the primary jet is deflected toward the opposite wall of the nozzle, generating a lateral force component and changing the direction of the resultant thrust vector. Previous studies [3] demonstrated that thrust-vector angles exceeding ten degrees can be achieved with secondary mass-flow ratios of only a few percent of the primary flow.

Despite extensive research on DTN configurations, the majority of studies have focused on steady-state flow conditions, considering axisymmetric and planar (2D/rectangular) nozzle geometries [3]. Early investigations, including work conducted at NASA Langley Research Center (NASA LaRC) [4–6], combined experiments and CFD (computational fluid dynamics) analyses to examine the influence of geometric parameters such as cavity shape, throat dimensions, and injection configuration on thrust vectoring performance. These studies systematically quantified key performance metrics, including thrust vectoring efficiency, primary nozzle discharge coefficient, and system resultant thrust ratio, and enabled the identification of near-optimal nozzle geometries for given operating conditions. Subsequent research further explored the sensitivity of steady flow solutions to geometric variations and operating parameters, as well as the role of uncertainties in shock location and flow structure [7], confirming that steady-state DTN behavior is now relatively well understood.

In contrast, investigations of unsteady and dynamic DTN behavior remain very limited. The numerical studies by Ferlauto and Marsilio introduced URANS (Unsteady Reynolds-Averaged Navier)-based analyses of DTN dynamics and highlighted the importance of characterizing the system response for control applications, including open- and closed-loop operation [8, 9]. However, experimental validation of these dynamic characteristics is scarce. The only known attempt to experimentally capture DTN dynamics was reported by Gu and co-workers, who observed pressure oscillations in the range of several kilohertz during transient operation [10]. Nevertheless, significant limitations in the experimental setup, including long pressure transmission lines and the application of aggressive low-pass filtering, raise concerns about the reliability of the measured data and the validity of the conclusions. As a result, the dynamic response of DTN systems remains experimentally largely unverified, and key characteristics such as response time, transient flow structure, and dominant oscillatory mechanisms are not yet well established.

The objective of the present study is therefore to experimentally investigate the dynamic behavior of a DTN and to identify the mechanisms responsible for non-stationary flow phenomena inside the nozzle. To the best of the authors' knowledge, this work represents the first dedicated experimental investigation of DTN dynamics.

EXPERIMENTAL SETUP

Test facility

The experiments were conducted using a test facility consisting of a test section - a DTN model - whose primary flow is driven by a Ludwieg Tube and whose secondary flow is supplied by a compressed-air system. The working medium is air, and the expansion occurs directly into the atmosphere.

A Ludwieg Tube is an apparatus that generates high-quality compressible flow with nearly constant stagnation conditions over a short test duration [11]. It operates based on the rapid expansion of compressed gas stored in a long reservoir tube, initiated by the opening of a fast-acting valve or rupture of a diaphragm that separates the

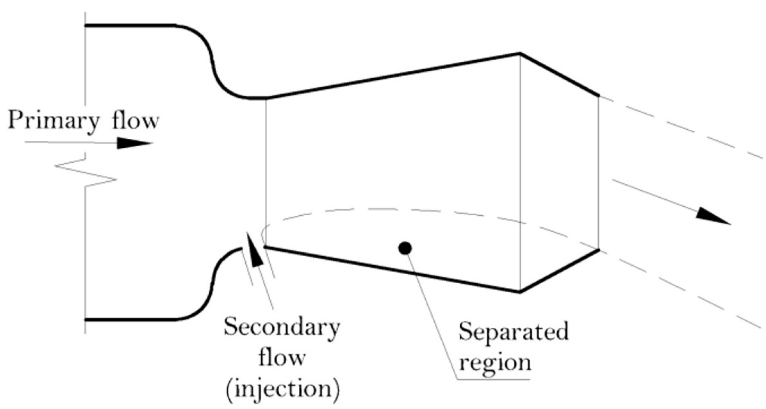

Figure 1. Dual-throat nozzle working principle

high-pressure driver section from the driven test section. Following diaphragm rupture or valve opening, an expansion wave propagates upstream into the driver tube, while a quasi-steady flow is established downstream in the test section, with mass flow limited by throat diameter in choked-flow conditions. The useful test window is determined by the travel time of the expansion wave along the reservoir tube. The driver tube used in this study consisted of 17 m of DN150 pipe, which corresponded to a 0.1 ms expansion wave cycle. The diaphragm, made of BoPET (biaxially oriented polyethylene) film, acted as a fast-opening valve when burst by a razor blade.

The secondary injection system was controlled independently by a direct-acting solenoid valve and an orifice plate. A diagram of the test stand, including the measurement points, is shown in Figure 2.

Dual-throat nozzle geometry

The investigated DTN geometry is based on the axisymmetric configuration originally proposed and experimentally validated by Deere and Flamm, named as the "13–60" geometry in their experimental studies [12] and the "202" configuration in the corresponding CFD analyses [4]. This configuration has been widely adopted as a reference case due to its high repeatability and well-documented steady-state performance characteristics.

Key geometric parameters were selected according to the reference Deere-Flamm configuration, which has been shown to provide a balance between thrust vectoring efficiency and discharge performance. This choice ensures comparability with previous studies while allowing a focused investigation of the dynamic response of the DTN system under controlled experimental conditions.

Figure 3 shows the characteristic dimensions, while the main geometric parameters are summarized in Table 1. The investigated DTN follows the axisymmetric Deere-Flamm reference configuration, reported as the "13–60" configuration in the experimental study and as configuration "202" in the corresponding CFD analyses [4,12].

The first (upstream) throat and middle part of the test section were produced using stereolithography, which made it possible to form the pressure gate channels. The second (downstream) throat was turned out of aluminum. The assembly of the complete section, including the transducers, is shown in Figure 4.

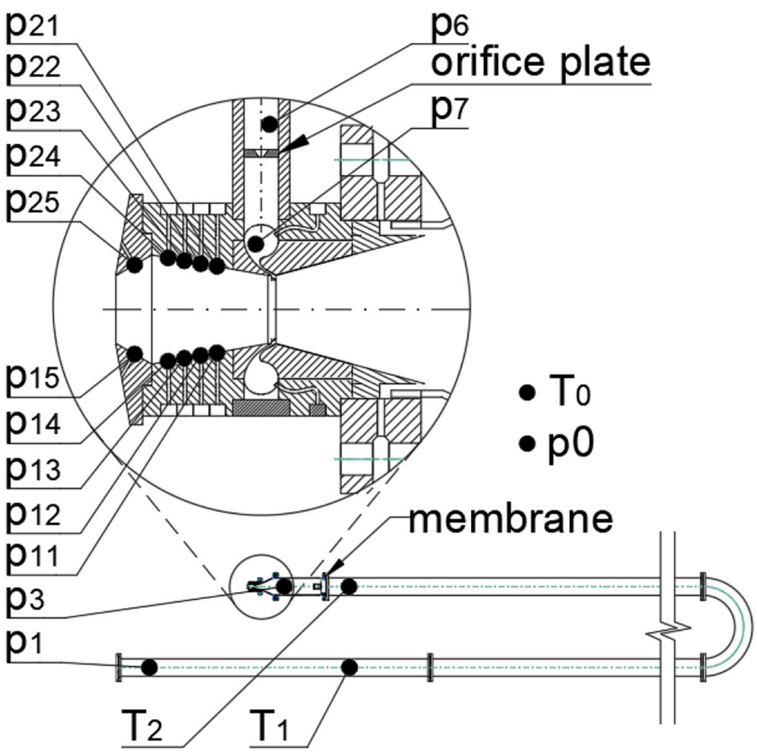

Figure 2. Test facility scheme with marked measurement points

Table 1. Main geometric parameters of the investigated DTN

Parameter	Symbol	Value
Upstream (primery) throat diameter	d_t	30 mm
Downstream throat diameter	d_e	30 mm
Upstream divergent-wall angle	Θ_1	20°
Downstream convergent-wall angle	Θ_2	60°
Cavity length	l	64 mm
Secondary injection angular span	φ_s	60°
Secondary injection angle	Θ_s	150°

Instrumentation

The experimental setup was equipped with a high-frequency pressure measurement system designed to capture transient flow phenomena inside DTN. The pressure signals were acquired simultaneously by National Instruments CompactRIO [13], with NI-9234 and NI-9237 modules operated in FPGA mode, at a sampling frequency of 51.2 kS/s per channel.

The wall-pressure instrumentation layout is summarized in Table 2. The axial coordinate x is measured from the upstream throat plane, positive downstream. Pressure taps p_{11}-p_{15} were located on the lower wall, whereas p_{21}- p_{25} were located on the upper wall. The selected layout provided measurements both in the cavity region and close to the downstream throat, where the pressure response is expected to be most sensitive to the development of asymmetric separation and jet deflection.

Kulite XTL-190 fast-response pressure transducers with a 380 kHz resonance frequency were used [14], ensuring sufficient temporal resolution to capture high-frequency flow oscillations observed in the kHz range. The measurement chain was designed to minimize dynamic distortion of the signal. In particular, the volume of the pressure transmission lines was minimized by placing transducers directly on the body of the test section.

All signals were recorded synchronously and referenced to the actuation signal of the secondary-flow control valve, which defined the temporal origin of the transient process. This approach enabled a consistent identification of key dynamic parameters, such as response delay and characteristic time scales of the system.

DATA PROCESSING AND ANALYSIS METHODS

Analysis of the dynamic response of the DTN system to activation of the secondary flow requires precise determination of time parameters, including delay time t_0, time constant τ, and asymptotic values of the signal y(t) – either wall pressure or secondary mass flow – before and after the change in flow conditions. The procedure consisted of three main steps: smoothing the signal using the Savitzky-Golay filter, defining a first-order model function with delay, and fitting the model function to the data by nonlinear regression. These methods were selected to ensure both immunity to high-pressure pulsations and correct interpretation of the physical phenomena occurring in the flow system.

The first step was to apply the Savitzky-Golay filter [15], a widely used technique for smoothing noisy data and computing derivatives without significantly distorting pulse shape or slope. The implementation was carried out using the Python scipy.signal library, which contains the savgol_filter tool [16].

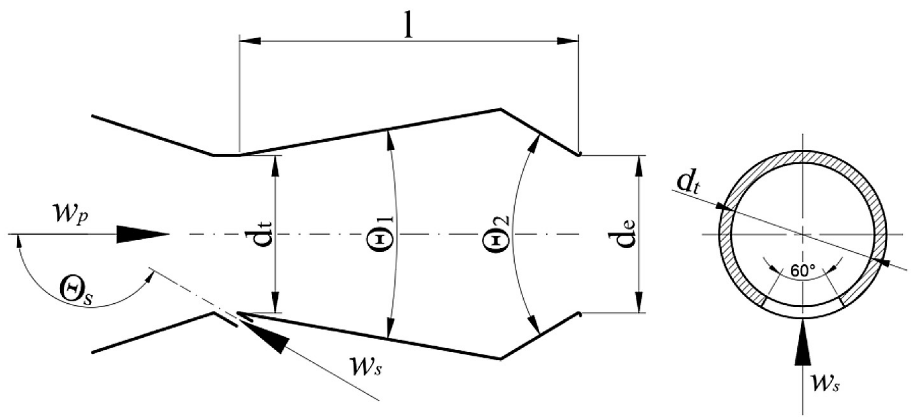

Figure 3. Dual-throat nozzle geometry

Table 2. Wall-pressure tap locations used in the DTN test section

Pressure tap	Wall	Axial position x, mm	Normalized position x/l
p_{11}	Lower	21.1	0.33
p_{12}		28.2	0.44
p_{13}		35.2	0.55
p_{14}		42.3	0.66
p_{15}		57.6	0.90
P_{21}	Upper	21.1	0.33
p_{22}		28.2	0.44
P_{23}		35.2	0.55
p_{24}		42.3	0.66
p_{25}		57.6	0.90

The sensitivity of the identified dynamic parameters to the Savitzky-Golay smoothing settings was additionally evaluated. The complete fitting procedure was repeated for several filter window lengths, while keeping the polynomial order constant. The tested window lengths covered the range from 251 to 1251 samples, corresponding to approximately 4.9–24.4 ms at the sampling frequency of 51.2 kS/s. The same first-order model with delay and the same fitting window were used in all cases.

The obtained values of the delay time and time constant varied only slightly within the tested range of smoothing parameters. For the representative pressure point p_{15}, the maximum relative variation of the identified time constant was below 10%, and the fitted response preserved the same delayed asymptotic character for all tested filter settings. Therefore, the identified response time was not considered to be an artifact of the selected Savitzky-Golay filter parameters.

The measured response to opening of the secondary-flow valve appears asymptotic and monotonic, which is typical for first-order systems with transport delay [17]. Accordingly, the following model was assumed:

$$y(t) = \begin{cases} y_0, & for: t < t_0, \\ y_\infty + (y_0 - y_\infty)\exp\left(-\dfrac{t-t_0}{\tau}\right), & for: t \geq t_0. \end{cases} \quad (1)$$

where: y_0 is the stable parameter value before the change (average from the "before" window), y_∞ is the stable parameter value after the change (average from the "after" window), t_0 is the transport delay, τ is the time constant.

The pre-transition and post-transition averaging windows were selected with regard to the operating characteristics of the Ludwieg Tube facility and the expected time scale of the DTN response. Since the useful test time of a Ludwieg

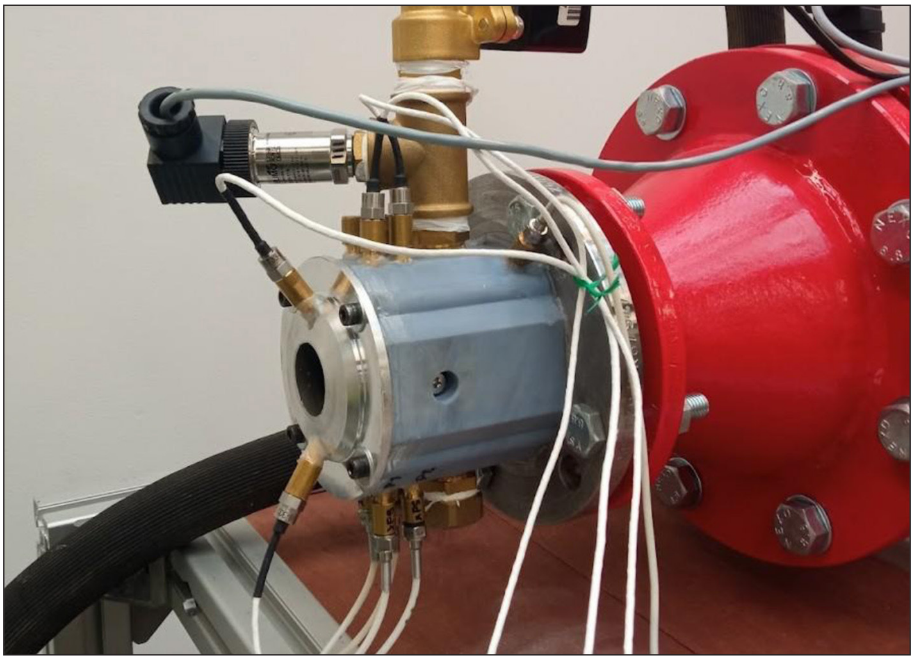

Figure 4. Test section facility

Tube is limited to the quasi-steady interval between the establishment of the flow and the arrival of waves reflected from the upstream reservoir, the averaging windows were placed only within portions of the record where the primary-flow conditions remained approximately constant. At the same time, safety margins were introduced between the averaging windows and the transient interval associated with secondary-flow actuation, so that the estimated values of (y_0) and (y_∞) were not affected by valve-opening dynamics, pressure-wave propagation, or the initial and final non-stationary parts of the test. The same window-selection rule was applied to all wall-pressure taps, which ensured that differences in fitted response parameters were caused by local nozzle-flow dynamics rather than by different processing assumptions (Figure 5).

The time constant τ is defined as the time, measured from t_0, at which the response reaches the fraction 1 - e^{-1} of the total change between y_∞ and y_0:

$$y(t_0 + \tau) = y_\infty + (y_0 - y_\infty)e^{-1} \tag{2}$$

Since the steady values y_0 and y_∞ were determined directly from the pre-transition ("before") and post-transition ("after") windows, only two model parameters had to be estimated from the smoothed signal. These parameters were collected in the ordered pair:

$$\theta = (t_0, \tau) \tag{3}$$

To fit the response model to the smoothed data, a Levenberg-Marquardt trust-region-reflective nonlinear fitting algorithm [18] was used via scipy.optimize.curve_fit [16]. The optimal ordered pair θ^* was obtained by minimizing the least-squares error between the smoothed measurement $\tilde{y}(t_i)$ and the model response $y(t_i; \theta)$:

$$\theta^* = \arg\min_{\theta} \sum_{i=1}^{N} \left(\tilde{y}(t_i) - y(t_i; \theta)\right) \tag{4}$$

The initial values and constraints selected in this way stabilized the fitting process and reduced the risk of solutions inconsistent with the physics of the system. After fitting, the residuals were inspected as the difference between the smoothed signal and the fitted response. No systematic drift was observed during the main transition, indicating that the delayed first-order model captured the dominant asymptotic behavior. The remaining residual structure was mainly related to high-frequency pressure oscillations, which were analyzed separately using FFT (fast Fourier transform).

The presented signal-processing method combines shape-preserving filtering, a model consistent with the physics of the phenomenon, and stable nonlinear fitting. As a result, the parameters t_0 and τ are resistant to noise and unambiguously describe system dynamics, allowing further analysis of the impact of flow conditions on the characteristics of the regulated flow.

EXPERIMENTAL RESULTS AND DISCUSSION

Flow conditions

Flow conditions set in the experiment are similar to those assumed by Flamm et al. for the mentioned earlier "13–60" geometry [12] and are as follows:

- Atmospheric pressure: p_0 = 101500 Pa
- Atmospheric temperature: T_0 = 290 K
- Upstream temperature: T_1 = 290 K
- Nozzle pressure ratio: NPR = p_3/p_0 = 2.8
- Primary mass flow: w_p = 0.45 kg/s
- Secondary mass flow: w_s = 0.014 kg/s
- Mass flow ratio: MFR = $w_s/(w_p + w_s) \times 100\%$ = 3%

Experiment results

Time analysis was performed for each pressure measurement point on the wall (Figure 2). The determined dimensionless time constants fell within the range from approximately 0.001 s to 0.002 s. It should be noted that for some points the pressure change was small, on the order of 0.08 bar. The longest response time constant was observed at point p_{15}, which was therefore selected as the representative limiting location for the response analysis. This point is located on the lower wall close to the downstream throat (x/l = 0.90), where the pressure field is strongly affected by the final development of asymmetric separation and by the resulting change in the effective sonic plane. From a control-oriented perspective, this location is critical because the slowest local pressure response determines the time required for the internal flow field to approach its new actuated state. The remaining wall-pressure taps showed

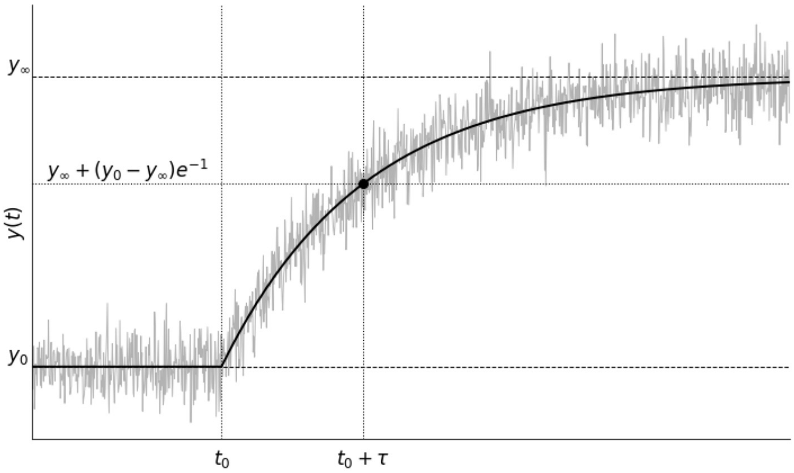

Figure 5. Parameters of first-order system with transport delay

the same delayed asymptotic response character, but with shorter time constants or smaller pressure changes; therefore, the behavior at p_{15} was consistent with the overall wall-pressure trends while representing the most conservative estimate of the nozzle response time. Figure 6 shows the pressure values measured at this point. Light blue represents raw values, while orange denotes the Savitzky-Golay-smoothed signal. Two horizontal dashed lines show the average pressure values in the "before" and "after" windows.

For comparison with CFD results, performed and reported by Ferlauto et al. [8], the same dimensionless time was added to the upper horizontal axis, defined as the ratio of time t [s] to the characteristic dimension l divided by the isentropic velocity $\sqrt{RT}$:

$$t^* = \frac{t}{l/\sqrt{RT}} \tag{5}$$

The same characteristic time scale $l/\sqrt{RT}$, was used consistently for all dimensionless time quantities reported in this study, including both the time axis t and the dimensionless time constant τ. Therefore, τ* was calculated using the same characteristic length l, gas constant R, and temperature T as in Equation 5.

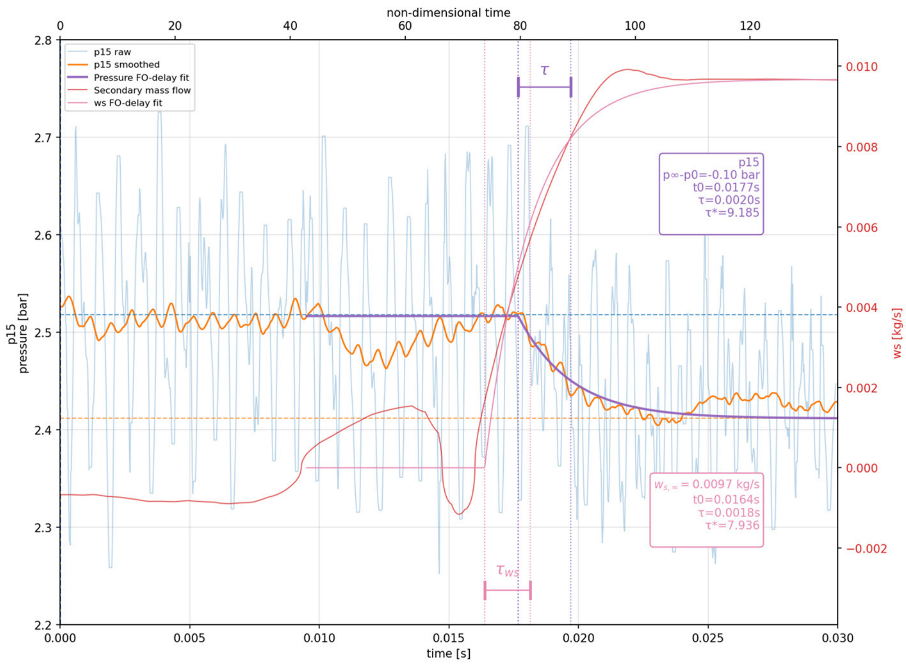

Figure 6. Raw and optimized values of p_{15} pressure and secondary mass flow ws

The optimized DTN impulse-response model is represented by a purple curve with vertical markers indicating the time-constant width τ = 0.002 s, or dimensionless τ^* = 9.19.

The red curve represents the secondary mass flow. The solenoid valve has its own dynamics, which are clearly visible in the data. Time t = 0 was set at the moment the signal was sent to the solenoid. To standardize the analysis and facilitate future comparisons, a time constant for valve dynamics was also determined using the method described in the previous section. In this case, the dimensionless time constant of the secondary-flow actuation system was τ^* = 7.94, indicated by pink vertical dotted lines. This value refers to the experimentally measured valve-secondary flow response. It is also worth noting that approximately 16 ms elapsed between the receipt of the signal and the actual beginning of valve opening.

Comparison with other studies

The most relevant comparison is with the CFD analyses conducted by Ferlauto and Marsilio [8,9], which also referred to DTN geometries designed at NASA LaRC. Their CFD-based dynamic response indicated a DTN time constant of the same order of magnitude, approximately τ^* = 14.2 for the analyzed configuration and actuation conditions. An important conclusion from their CFD analysis was that the DTN flow field exhibits complex, nonlinear dynamic behavior resulting from strong interactions among moving shock waves, boundary layers, and separated-flow regions. This led those authors to focus more on overall performance, control, and system setup than on precise identification of time constants. This confirms that the experimentally identified time scale is consistent, at least in order of magnitude, with the available numerical studies.

It should be emphasized that the quantitative values of the identified delay time and time constant are valid for the investigated operating point. Higher NPR values were not considered in the present study because, for DTN configurations, they are associated with a significant decrease in propulsion efficiency due to increasingly unfavorable expansion behavior. Changes in NPR, secondary mass-flow ratio, or actuator dynamics may affect the separation pattern, shock structure, and pressure recovery inside the cavity. Therefore, the present results should be interpreted as an experimentally identified dynamic response for a representative operating condition, rather than as a complete dynamic map of the DTN.

Non-stationary behavior

The phenomenon of unsteady flow was first identified by Gu et al. [10] and later studied using CFD by Wang et al. [19]. In the present study, these oscillations were not identified only qualitatively from the time histories, but were evaluated quantitatively in the frequency domain using FFT analysis of the wall-pressure signals. The resulting spectra are shown in Figure 7, where the dominant pressure-pulse frequencies can be clearly distinguished. For different wall points, the main frequencies vary slightly, but always occur around 1000–3000 Hz. For example, at point p_{15} the pulsations reached around 1285 Hz before secondary-flow injection and 1429 Hz after injection, with an amplitude of approximately 0.05 bar. Because these components were observed at wall-pressure locations and were present outside the short valve-opening interval, they are attributed

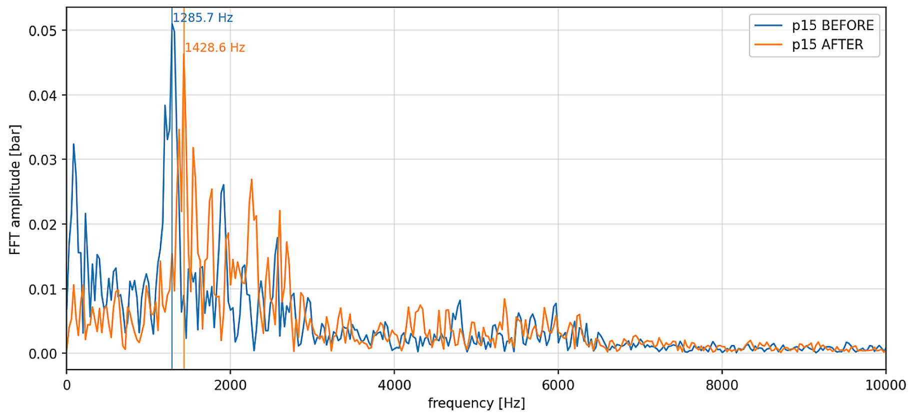

Figure 7. Results of FFT analysis for p_{15} point

mainly to internal nozzle-flow dynamics rather than to the valve actuation alone. In particular, shock-separation interaction and unsteady cavity flow are considered the most likely sources, although some contribution from the secondary-injection and upstream supply systems cannot be fully excluded without additional dedicated measurements. Only an analysis of the control system, with the entire aircraft as the object of control, can determine whether this phenomenon is critical and constitutes an obstacle or not.

CONCLUSIONS

This study presented an experimental investigation of the dynamic response of an axisymmetric dual-throat nozzle under real transient secondary-flow actuation. The results help address a gap in the available DTN literature, where steady-state performance has been studied extensively while experimentally determined dynamic characteristics have remained limited. High-frequency wall-pressure measurements allowed transient evolution of the flow to be captured and the response of the nozzle system to be assessed in time-resolved form.

The performed time-domain analysis showed that the DTN response can be described, to first order, by a delayed asymptotic model. For the investigated operating conditions, the longest and most representative response was observed at point p_{15}, for which the dimensionless time constant was determined as $\tau^* = 9.19$. The identified delay time and time constant may be used as parameters of a control-oriented reduced-order model for response-time prediction, actuator bandwidth estimation, and preliminary controller tuning. For example, for a 1 m long nozzle with an exhaust gas temperature of 1000 K, the response time would be less than 0.02 s, which is faster than the response time of movable control surfaces.

The measurements also confirmed that internal DTN flow is not fully stationary and that transient operation is accompanied by measurable pressure fluctuations. Future work should extend the experiment to a wider range of NPR and secondary mass-flow ratios, include direct thrust-vector angle measurements, and use faster secondary-flow actuation to better separate nozzle-flow dynamics from valve dynamics. Such data would allow the development of operating-envelope-dependent reduced-order models for DTN control applications.

REFERENCES

1. Deere K.A. Summary of fluidic thrust vectoring research conducted at NASA Langley Research Center. In: 21st AIAA Applied Aerodynamics Conference; 2003 Jun 23–26; Orlando, FL, USA. Reston: AIAA; 2003. AIAA Paper 2003–3800. https://doi.org/10.2514/6.2003-3800
2. Afridi S., Khan T.A., Shah S.I.A., Shams T.A., Mohiuddin K., Kukulka D.J. Techniques of fluidic thrust vectoring in jet engine nozzles: a review. Energies. 2023; 16(15): 5721. https://doi.org/10.3390/en16155721
3. Deere K.A., Berrier B.L., Flamm J.D., Johnson S.K. A computational study of a new dual throat fluidic thrust vectoring nozzle concept. In: 41st AIAA/ASME/SAE/ASEE Joint Propulsion Conference & Exhibit; 2005 Jul 10–13; Tucson, AZ, USA. Reston: AIAA; 2005. AIAA Paper 2005–3502. https://doi.org/10.2514/6.2005-3502
4. Deere K.A., Flamm J.D., Berrier B.L., Johnson S.K. Computational study of an axisymmetric dual throat fluidic thrust vectoring nozzle for a supersonic aircraft application. In: 43rd AIAA/ASME/SAE/ASEE Joint Propulsion Conference & Exhibit; 2007 Jul 8–11; Cincinnati, OH, USA. Reston: AIAA; 2007. AIAA Paper 2007–5085. https://doi.org/10.2514/6.2007-5085
5. Flamm J.D., Deere K.A., Berrier B.L., Johnson S.K., Mason M.L. Experimental study of a dual-throat fluidic thrust-vectoring nozzle concept. In: 41st AIAA/ASME/SAE/ASEE Joint Propulsion Conference & Exhibit; 2005 Jul 10–13; Tucson, AZ, USA. Reston: AIAA; 2005. AIAA Paper 2005–3503. https://doi.org/10.2514/6.2005-3503
6. Flamm J.D., Deere K.A., Mason M.L., Berrier B.L., Johnson S.K. Design enhancements of the two-dimensional, dual throat fluidic thrust vectoring nozzle concept. In: 3rd AIAA Flow Control Conference; 2006 Jun 5–8; San Francisco, CA, USA. Reston: AIAA; 2006. AIAA Paper 2006–3701. https://doi.org/10.2514/6.2006-3701
7. Chen Q.Y., Gottlieb D., Hesthaven J.S. Uncertainty analysis for the steady-state flows in a dual throat nozzle. J. Comput. Phys. 2005; 204(2): 378–398. https://doi.org/10.1016/j.jcp.2004.10.019
8. Ferlauto M., Marsilio R. Open and closed-loop responses of a dual-throat nozzle during fluidic thrust vectoring. In: 52nd AIAA/SAE/ASEE Joint Propulsion Conference; 2016 Jul 25–27; Salt Lake City, UT, USA. Reston: AIAA; 2016. AIAA Paper 2016–4504. https://doi.org/10.2514/6.2016-4504
9. Ferlauto M., Marsilio R. Numerical investigation of the dynamic characteristics of a dual-throat nozzle for fluidic thrust-vectoring. AIAA J. 2017; 55(1): 86–98. https://doi.org/10.2514/1.J055044

10. Gu R., Xu J. Dynamic experimental investigations of a bypass dual throat nozzle. J. Eng. Gas Turbines Power. 2015; 137(8): 084501. https://doi.org/10.1115/1.4029391
11. Ludwieg H. Ein neues Verfahren für intermittierend betriebene Hochgeschwindigkeits-Windkanäle. Göttingen: Aerodynamische Versuchsanstalt Göttingen; 1955. Technical report. German.
12. Flamm J.D., Deere K.A., Mason M.L., Berrier B.L., Johnson S.K. Experimental study of an axisymmetric dual throat fluidic thrust vectoring nozzle for supersonic aircraft application. In: 43rd AIAA/ASME/SAE/ASEE Joint Propulsion Conference & Exhibit; 2007 Jul 8–11; Cincinnati, OH, USA. Reston: AIAA; 2007. AIAA Paper 2007–5084. https://doi.org/10.2514/6.2007-5084
13. National Instruments. NI cRIO-9024 series resource. Austin: National Instruments; 2024. Available from: https://www.ni.com/docs/en-US/bundle/crio-9024-seri/resource/375233f.pdf (Accessed: 03.08.2024).
14. Kulite Semiconductor Products, Inc. XTL-190 miniature pressure transducer. Leonia: Kulite Semiconductor Products, Inc.; 2022. Available from: https://kulite.com/assets/media/2022/09/XTL-190-1.pdf (Accessed: 03.08.2024).
15. Savitzky A., Golay M.J.E. Smoothing and differentiation of data by simplified least squares procedures. Anal. Chem. 1964; 36(8): 1627–1639. https://doi.org/10.1021/ac60214a047
16. Virtanen P., Gommers R., Oliphant T.E., Haberland M., Reddy T., Cournapeau D., et al. SciPy 1.0: fundamental algorithms for scientific computing in Python. Nat. Methods. 2020; 17: 261–272. https://doi.org/10.1038/s41592-019-0686-2
17. Seborg D.E., Edgar T.F., Mellichamp D.A., Doyle F.J. Process dynamics and control. 4th ed. Hoboken: John Wiley & Sons; 2017.
18. Gavin H.P. The Levenberg–Marquardt algorithm for nonlinear least squares curve-fitting problems. Durham: Department of Civil and Environmental Engineering, Duke University; 2024. Technical report. Available from: https://people.duke.edu/~hpgavin/ce281/lm.pdf (Accessed: 13.02.2026).
19. Wang Y.S., Xu J.L., Huang S. Study of starting problem of axisymmetric divergent dual throat nozzle. J. Eng. Gas Turbines Power. 2017; 139(6): 062602. https://doi.org/10.1115/1.4035230